SANDIA REPORT
SAND2006-2664
Unlimited Release
Printed June 2006

Investigation of Temporal Contrast Effects in Femtosecond Pulse Laser Micromachining of Metals

Jeremy A. Palmer, Benjamin R. Campbell

Prepared by
Sandia National Laboratories
Albuquerque, New Mexico 87185, and Livermore, California 94550

Sandia is a multiprogram laboratory operated by Sandia Corporation, a Lockheed Martin Company, for the United States Department of Energy's National Nuclear Security Administration under Contract DE-AC04-94AL85000.

Issued by Sandia National Laboratories, operated for the United States Department of Energy by Sandia Corporation.

Available to DOE and DOE contractors from
U.S. Department of Energy
Office of Scientific and Technical Information
P.O. Box 62
Oak Ridge, TN 37831

Telephone: (865) 576-8401
Facsimile: (865) 576-5728
E-Mail: reports@adonis.osti.gov
Online ordering: http://www.osti.gov/bridge

Available to the public from
U.S. Department of Commerce
National Technical Information Service
5285 Port Royal Rd.
Springfield, VA 22161

Telephone: (800) 553-6847
Facsimile: (703) 605-6900
E-Mail: orders@ntis.fedworld.gov
Online order: http://www.ntis.gov/help/ordermethods.asp?loc=7-4-0#online

SAND 2006-2664
Unlimited Release
Printed June 2006

Investigation of Temporal Contrast Effects in Femtosecond Pulse Laser Micromachining of Metals

Phase I Final Technical Report

WFO-NFE Funds-In Agreement Number 141040901

Jeremy A. Palmer, Ph.D., P.E.
Meso Manufacturing and Systems Development Department
Sandia National Laboratories
P.O. Box 5800
Albuquerque, NM 87185-1245, U.S.A.

Benjamin R. Campbell
The Pennsylvania State University Electro Optics Center
222 Northpointe Blvd.
Freeport, PA 16229, U.S.A.

Abstract

Femtosecond pulse laser drilling has evolved to become a preferred process for selective (maskless) micromachining in a variety of materials, including metals, polymers, semiconductors, ceramics, and living tissue. Manufacturers of state-of-the-art femtosecond laser systems advertise the inherent advantage of micromachining with ultra short pulses: the absence of a heat affected zone. In the ideal case, this leads to micro and nano scale features without distortion due to melt or recast. However, recent studies have shown that this is limited to the low fluence regime in many cases. High dynamic range autocorrelation studies were performed on two commercial Ti:sapphire femtosecond laser systems to investigate the possible presence of a nanosecond pedestal in the femtosecond pulse produced by chirped pulse amplification. If confirmed, nanosecond temporal phenomena may explain many of the thermal effects witnessed in high fluence micromachining. The material removal rate was measured in addition to feature morphology observations for percussion micro drilling of metal substrates in vacuum and ambient environments. Trials were repeated with proposed corrective optics installed, including a variable aperture and a nonlinear frequency doubling crystal. Results were compared. Although the investigation of nanosecond temporal phenomena is ongoing, early results have confirmed published accounts of higher removal rates in a vacuum environment.

Acknowledgment

The authors are grateful to Mr. Jeff Thomas of the Pennsylvania State University Electro Optics Center for his support of this research.

Contents

Figures..... 6
Tables..... 7
Introduction..... 9
Procedure..... 11
Results..... 14
Conclusions and Future Work..... 17
References..... 18
Appendix A: Test Schedules...... 19
Appendix B: Substrate Legends..... 20

Figures

1. (a) M^2 characterization apparatus (close-up): (1) turning mirror, (2) lens, (3) camera, (b) optical system view showing femtosecond laser (right top)…….. 11

2. (a) Apparatus for percussion drilling of holes with through hole detection in vacuum and ambient conditions, (b) close-up showing hole array…..……. 12

3. Apparatus for percussion drilling at the second harmonic…….……..…….…. 13

4. CCD image of the Hurricane laser spot 10 cm from the lens (25 cm focal length) …….. 14

5. Material removal rate versus pulse energy for aluminum…….…. 15

6. Material removal rate versus pulse energy for stainless steel…… 15

7 Material removal rate versus pulse energy for copper……... 16

8 (a) SEM image of array surface (0.076 mm Al, vacuum, 211 μJ/pulse, col 11-15), (b) cross-section of a typical hole…… 16

9 Comparison of holes percussion drilled in stainless steel with and without an aperture inserted in the optical path. In each picture, the hole drilled with the aperture is at the right. (a) Before cleaning, some asymmetry is noted in the debris. (b) After cleaning…... 17

B.1 Substrate legend for percussion drilling experiments: each label designates the location of an array relative to the reference mark, run at the prescribed pulse energy…….. 23

B.2 Substrate legend for percussion drilling experiments at the second harmonic: each label designates the location of an array relative to the reference mark, run at the indicated pulse energy……... 23

Tables

1. Airy Disk Diameter Data…….. 14
A.1 Percussion Drilling Test Schedule……. 19
A.2 Test Schedule for Percussion Drilling at the Second Harmonic…… 22

This page intentionally left blank.

Investigation of Temporal Contrast Effects in Femtosecond Pulse Laser Micromachining of Metals

Jeremy Palmer, Ben Campbell

1.0 Introduction

Femtosecond pulse laser drilling has evolved to become a preferred process for selective (maskless) micromachining in a variety of materials, including metals, polymers, semiconductors, ceramics, and living tissue. Because the ultrashort pulse duration is often shorter than the rate of heat transfer in the substrate, micromachining with femtosecond pulses is characterized by the absence of a heat affected zone. In the ideal case, this leads to micro and nano scale features that are free of distortion caused by molten material ejected from the ablation site. However, recent studies suggest that this benefit is limited to the low fluence regime in many cases (Campbell, Semak, and Thomas) [1]. Micromachining at higher fluence reveals familiar thermal effects. This situation negatively impacts the throughput and ultimately the cost of femtosecond laser manufacturing operations. In a 1998 study of ultrashort systems with chirped pulse amplification (CPA) Nantel *et al.* suggest the presence of a nanosecond pedestal prior to the femtosecond portion of the pulse that may contribute to the high fluence thermal effects (Nantel *et al.*, 1998) [2]. The ratio of the peak intensity of the femtosecond pulse and the nanosecond pedestal is referred to as the *intensity contrast ratio* (ICR) [2]. Poor contrast in CPA lasers is attributable to several causes such as misaligned optics, spectral clipping and phase distortion, and amplified stimulated emission (ASE) background [2]. Several groups have proposed remedies, the least costly of which include frequency doubling, installing a hard intra cavity aperture, or a fast saturable absorber such as a gallium arsenide plate (Curley, Darpentigny, Cheriaux, Chambaret, and Antonetti, 1995) [3, 2]. These corrective measures were evaluated in this project. Although it is one of the easiest to implement, introducing a nonlinear frequency doubling crystal in the optical system has the disadvantage of inefficient conversion which robs the system of energy [2].

Verifying the nanosecond component is difficult due to the high dynamic range and temporal resolution required to capture high ICR nano and femtosecond events simultaneously. Braun *et al*. devised a phased-matched scanning autocorrelation technique to characterize the femtosecond pulse of a Kerr-lens mode-locked Ti:sapphire laser operating at 780 nm, 300mW; similar to the system used in this research (Braun *et al*.,1995) [4]. Inspection of the autocorrelation trace revealed a pedestal that decayed exponentially over 1.5 ps [4]. The reader is referred to [4] for complete details. Konoplev utilized frequency conversion to realize a second-order autocorrelator with dynamic range of approximately twelve orders of magnitude and 50 femtosecond temporal resolution (Knopolev, 2000) [5]. This work confirmed that loss mechanisms that contributed to pulse broadening and poor ICR could be reduced by introducing a GaAs plate prior to final compression of the amplified ultrashort pulse [5].

The Two Temperature Model (TTM) is useful in predicting the minimum laser fluence that causes ablation in a given material (the ablation threshold or threshold fluence) and its dependence on pulse duration (Furusawa *et al.*, 1999; Chichkov *et al.*, 1996; Wellershoff, Hohlfeld, Güdde, and Matthias, 1999) [6, 7, 8]. The TTM relates the electron (*e*) and lattice (*i*) temperatures to one-dimensional heat transfer in the substrate [7]:

$$C_e \frac{\partial T_e}{\partial t} = -\frac{\partial Q(z)}{\partial z} - \gamma(T_e - T_i) + S, \tag{1}$$

$$C_i \frac{\partial T_i}{\partial t} = \gamma(T_e - T_i), \tag{2}$$

$$Q(z) = -k_e \frac{\partial T_e}{\partial z}, \tag{3}$$

$$S = I(t) A \alpha(\exp(-\alpha z)). \tag{4}$$

The heat capacity per unit volume is denoted by C (J/m^3·K) and T is absolute temperature (K) [7]. Heat flux (W/m^2) in the normal direction (z) into the substrate is represented by Q in (1) and (3). Electron thermal conductivity is given by k_e in (3). The constant γ quantifies the degree of electron-phonon (lattice) coupling in the system [6, 7]. It is often a source of uncertainty in the model, and must be determined by reliable experimental methods (Corkum, Brunel, and Sherman, 1988) [9]. Laser heating is described by S in (1) and (4), where $I(t)$ is the irradiance (J/m^2·s), A is the surface transmissivity, and α is the material absorption coefficient (attenuation coefficient) (Hecht, 2002) [10, 7].

In the femtosecond regime, the pulse duration is much less than the electron cooling time [7]. This condition allows simplifying assumptions (most importantly, electron-phonon coupling is neglected) that lead to the following expression for the greatest lattice temperature after absorption of the pulse (see [7] for complete details):

$$T_i = \frac{F_a \alpha}{C_i} \exp(-\alpha z), \tag{5}$$

where F_a is the absorbed fluence given by the product of the irradiance and the pulse duration [7]. Ablation occurs when the following condition is satisfied:

$$C_i T_i \geq \rho c_{p_{vap}} \Delta T_i, \tag{6}$$

where ρ is the density (kg/m^3) and c_{pvap} is the specific heat of vaporization (J/kg·K) [7]. It follows that (5) and (6) can be used to estimate the threshold fluence for a given material in the femtosecond regime. Another useful approximation of threshold fluence valid in the femtosecond regime is given by [7]:

$$F_{th} \cong \frac{\rho c_{p_{vap}}}{\alpha}. \tag{7}$$

From the TTM in the femtosecond regime, it is evident that heat transfer to the lattice occurs on a picosecond time scale that is much longer than the pulse duration [7]. Thus, we conclude that micromachining with femtosecond pulses should be characterized by a direct solid to vapor phase change without evolution of molten material [6, 7, 8]. However, recent studies have

clearly shown melting and recast effects at fluence levels much greater than the ablation threshold [1]. This observation has led the hypothesis that at high fluence, the pure femtosecond pulse acquires a nanosecond component (pedestal) that represents a significant portion (20% or greater) of the pulse energy (Semak, Thomas, and Campbell, 2004) [11, 1].

The objectives of this program are the following. The first objective is to use high dynamic range autocorrelation techniques to confirm the nanosecond pedestal in two commercial Ti:sapphire femtosecond lasers. The system associated with the data in this report is a Spectra Physics Hurricane® located at Sandia National Laboratories. The Hurricane operates at a wavelength of 800 nm with 1 kHz repetition rate and peak pulse energy greater than 750 μJ. Pulse width is slightly longer than 100 fs (Spectra Physics, 2004) [12]. The output beam exhibits horizontal linearly polarized [12]. The second objective is to study the effects of the nanosecond pedestal on laser-matter interaction in the femtosecond regime. This report documents activities associated with the final objective: to perform experimental trials to evaluate the effect of improving ICR by frequency doubling. The evaluation is based on measurements of the material removal rate and quality (i.e. feature accuracy and the presence of recast material) of percussion drilled features in various metallic substrates. Trials were conducted in ambient and vacuum environments.

2.0 Procedure

2.1 Beam Characterization

Measurements of the diameter of the Hurricane beam at sequential positions along the optical path were conducted to in support of efforts to characterize the times-diffraction-limit factor (M^2), an invariant measure of beam quality (ISO, 1999) [13]. The procedure described below implicitly captures the three parameters required for characterization of a beam with radial symmetry including the location and diameter of the beam waist, and the far-field divergence angle [13].

Fig. 1 depicts the M^2 measurement apparatus. The apparatus consists of a right angle

(a) **(b)**

Fig. 1. (a) M^2 characterization apparatus (close-up): (1) turning mirror, (2) lens, (3) camera, (b) optical system view showing femtosecond laser (right top).

mirror, a 250-mm focal length bi-convex lens, and a CCD camera mounted to the graduated rail system shown. The camera is a Lumenera Lu120C color CCD with 6.7-micrometer square pixels. The beam was attenuated to the minimum power of approximately 340 μW throughout the trial. A variable polarizer was not included in the optical path in order to preserve the nominal polarization state of the laser. A variable aperture was included to clip the "tails" off the incoming beam and make the intensity distribution radially uniform. The focusing optic was set at the 1 cm position on the rail and images were captured at 2 cm increments from 8-40 cm from the focusing optic. Images were exported to a MATLAB® script that measured the pixel intensity in the *x* and *y* directions for the Cartesian coordinate system mapped to the center of the spot. Intensity data was subsequently normalized to the highest measured value, and the $1/e^2$ beam diameter determined.

In late 2004, a temporal characterization of the Hurricane pulse was performed. Measurements with a Femtochrome FR103PD scanning autocorrelator revealed a temporal pulse width of 127.5 fs.

2.2 Percussion Drilling with Through-Hole Detection

The Sandia femtosecond laser micromachining system includes a chamber for laser operations in a vacuum environment. Vacuum operations were conducted at pressure between 1 and 3 Torr. The apparatus shown in Fig. 2 was constructed for percussion drilling of holes in metal substrates. The laser beam passes through a calcium fluoride window in the top of the

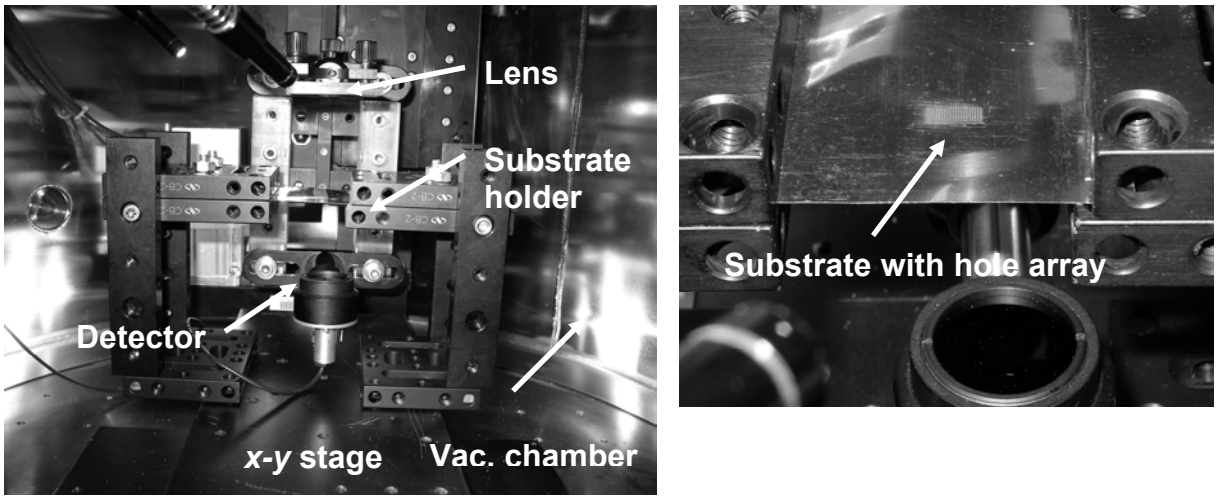

Fig. 2. (a) Apparatus for percussion drilling of holes with through hole detection in vacuum and ambient conditions, (b) close-up showing hole array.

vacuum chamber and is focused onto the metal substrate (see Fig. 2a). The substrate is suspended between two clamps attached to an *x*-*y* stage assembly at the chamber floor. A computer program coordinates operation of the laser's electromechanical shutter and *x*-*y* stage to create a series of hole arrays similar to the one shown in Fig. 2b. At the start of the micromachining trial, the system controller opens the shutter (thereby exposing the substrate to the beam). Next, the system simultaneously translates the lens (and thus the focal point of the beam) in the (vertical) *z* direction, and the substrate in the (horizontal) *x* direction. This action

results in micromachining of a narrow trench in the substrate, the width of which is reduced near the beam waist or focal point. The substrate and lens are subsequently returned to positions corresponding to the start of the trench. The system proceeds to percussion drill a column of ten holes extending rearward (in the y direction) from that point (see Fig. 2b). Indexing to the next hole in the column occurs when laser light is detected below the substrate. The controller records the drill time in milliseconds. Drill times for the ten holes are ultimately compiled to yield the average material removal rate. This sequence is repeated at regular spatial intervals for a total of twenty columns and two hundred holes. Each column is drilled at a different focal position that matches the focal position at that point along the trench. If the laser doesn't break through within a prescribed time limit, the system indexes to the next hole. Drilling of a particular column is terminated after a predetermined number of time outs. Average material removal rate data for each column is compared. The greatest rate is ultimately used in a calculation of material removal rate per pulse.

Multiple arrays were drilled on substrates with varying laser pulse energy, and alternating environment. The schedule of tests is listed in Appendix A. Following the testing, selected rows of holes within the arrays on each substrate were sectioned, mounted, and polished. Scanning electron microscopy (SEM) was employed to capture photo micrographs of the sectioned holes, revealing wall geometry and recast layer features.

2.3 Percussion Drilling at the Second Harmonic

The percussion drilling apparatus shown in Fig. 2 was expanded to include a barium borate (BBO) crystal and filter. These optics were installed upstream of the lens as depicted below.

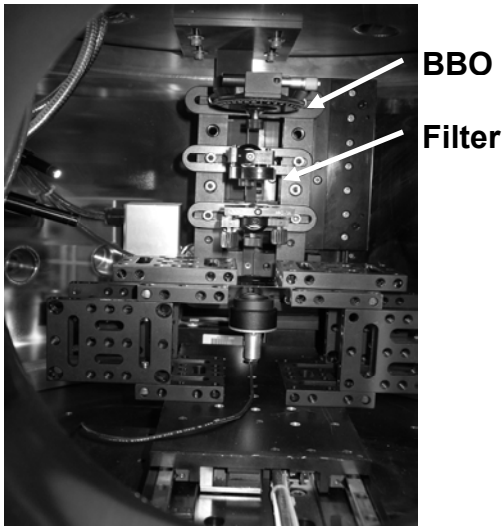

Fig. 3. Apparatus for percussion drilling at the second harmonic.

Light exiting the BBO is doubled in frequency, thus changing the wavelength from 800 nm to 400 nm. A UV filter was added to remove any remnant of the first harmonic (see Fig. 3). A commercial filter that was exactly matched to the 400 nm wavelength was unavailable. Consequently, some low-intensity 800 nm light was observed at the exit of the filter. The previous percussion drilling program was repeated in the trials listed in Appendix A, Table A.2. Note that in the second harmonic trials, the pulse energies listed in Table A.2 were multiplied by a factor of 1.47 to compensate for losses in the crystal and filter. In an effort to improve the

symmetry of the spatial energy distribution in the laser spot (see Section 3.2), an aperture was added to the optical path to clip the "tails" that were observed in the peripheral segments of the defocused beam.

Results

3.1 Beam Characterization

Table 1 lists results of CCD camera measurements of the $1/e^2$ spot diameter versus distance from the focusing objective. Despite the high attenuation, the beam intensity at the center of the

Table 1. Airy Disk Diameter Data

Distance from Lens (cm)	*X* Diameter (pixels)	*Y* Diameter (pixels)
8	545	556
10	497	508
12	450	455
14	403	406
16	362	371
18	316	319
20	269	274
22	227	235
24	181	179
26	134	139
28	95	127
30	91	115
32	121	149
34	172	192
36	211	237
38	269	289
40	315	328

spot was consistently great enough to saturate the camera. A typical spot is pictured in Fig. 4.

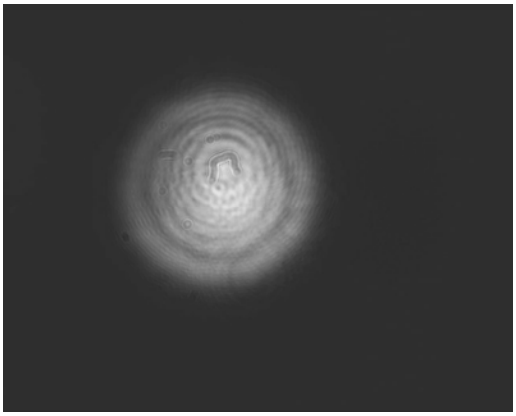

Fig. 4. CCD image of the Hurricane laser spot 10 cm from the lens (25 cm focal length)

The area of saturation was more pronounced near focus. At an arbitrary distance before the lens, the measured beam diameters were 680 pixels (x) and 703 pixels (y). Work is ongoing to process the beam diameter data in calculations of M^2.

3.2 Percussion Drilling with Through-Hole Detection

Figures 5, 6, and 7 are plots of peak material removal rate per pulse versus pulse energy for aluminum, stainless steel, and copper substrates. Each plot confirms the published observations

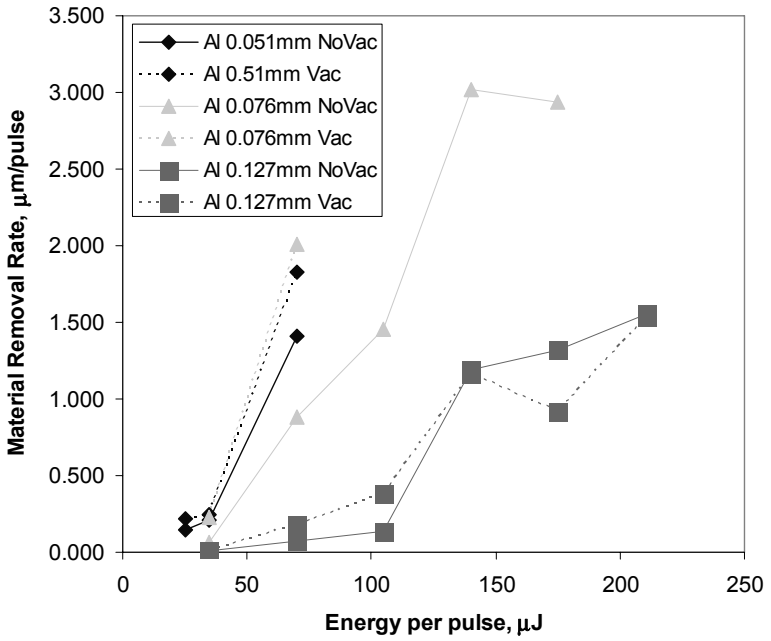

Fig. 5. Material removal rate versus pulse energy for aluminum.

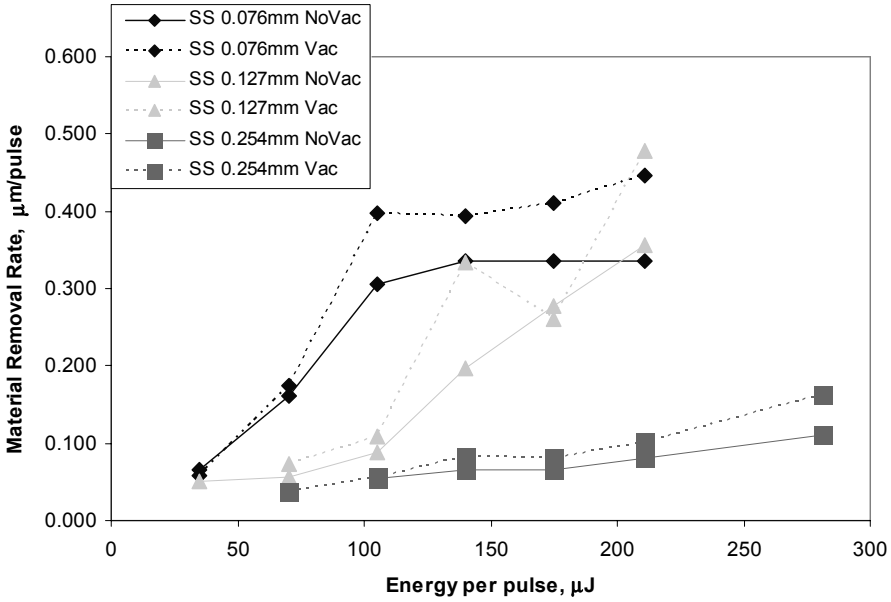

Fig. 6. Material removal rate versus pulse energy for stainless steel.

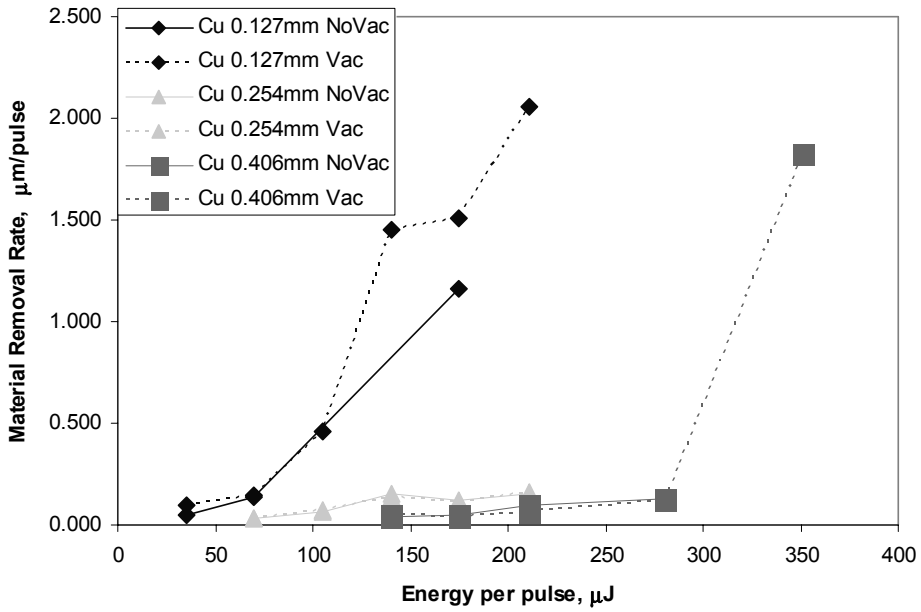

Fig. 7. Material removal rate versus pulse energy for copper.

that material removal rate (1) increases with pulse energy and, (2) is higher in vacuum in many cases (Dausinger, 2003) [14]. The greatest removal rates were observed in aluminum.

Fig. 8a is a SEM image of the surface of a portion of an array drilled in 0.076 mm thick aluminum in a vacuum. Beam energy was 211 µJ/pulse. Fig. 8b is a cross section of a typical hole. The images clearly show errors in the intended circular geometry of the feature. Recast and molten material is less apparent. It is unclear if the error is due to secondary thermal effects at high fluence due to the presence of a pedestal in the pulse, error in the spatial distribution of the focal spot, polarization effects, or a combination of these and other phenomena. The images

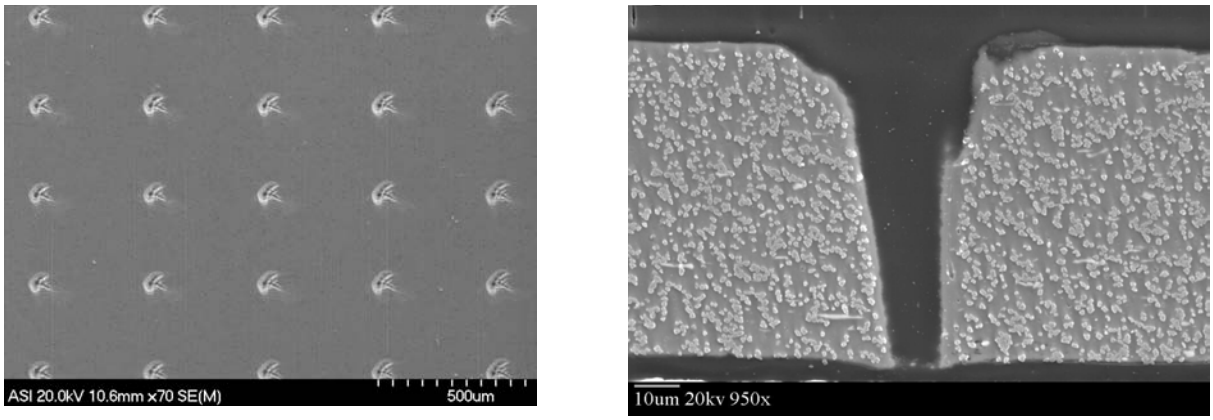

(a) **(b)**

Fig. 8. (a) SEM image of array surface (0.076 mm Al, vacuum, 211 µJ/pulse, col. 11-15), (b) cross-section of a typical hole.

are a basis of comparison to drilling performed at the second harmonic with the identical substrate

3.3 Percussion Drilling at the Second Harmonic

At the time of publication, processing of second harmonic drilling data was ongoing. Fig. 9 is a side-by-side comparison of holes drilled with and without the aperture. Inspection of

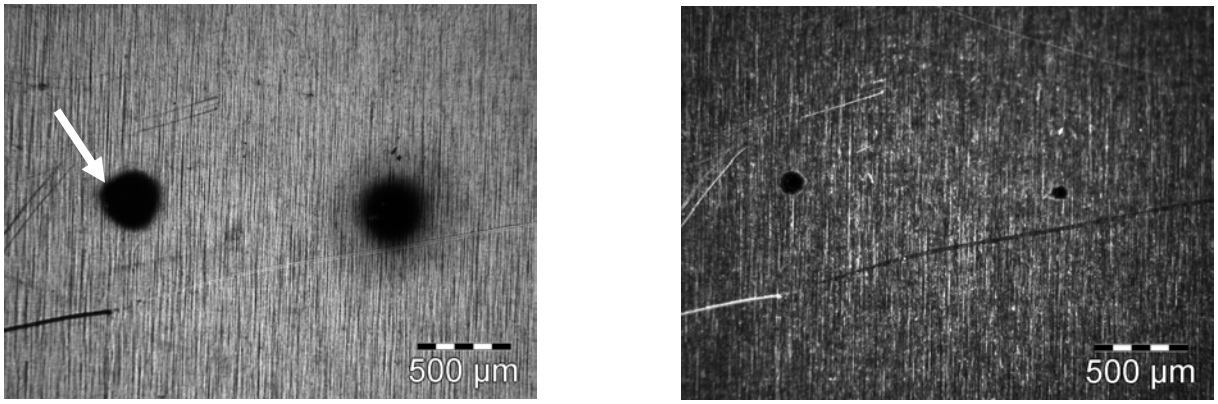

(a) **(b)**

Fig. 9. Comparison of holes percussion drilled in stainless steel with and without an aperture inserted in the optical path. In each picture, the hole drilled with the aperture is at the **right**. (a) Before cleaning, some asymmetry is noted in the debris. (b) After cleaning.

Fig. 9a reveals slight asymmetry in the pattern of debris surrounding the hole drilled without the aperture (left). The debris pattern of the hole drilled with the aperture (right) exhibits more radial symmetry. Cleaning (Fig. 9b) reveals that the hole drilled with the aperture is smaller and contains errors in roundness and a "tail," perhaps induced by polarization (Nolte et al., 1999) [15]. Similar results were obtained in two subsequent trials. Spatial effects similar to those discussed in Section 3.2 were not observed.

Conclusions and Future Work

An experimental program is ongoing to study temporal contrast effects in femtosecond pulse laser micromachining of metals. To date, percussion drilling trials have confirmed published observations that material removal rate is higher with increasing energy per pulse and vacuum environment. SEM images of hole arrays drilled at high fluence clearly show feature errors. However, it is unclear if the nanosecond pedestal is the root cause. Trials performed in 0.076 mm aluminum substrates are a basis of comparison for trials run with the frequency doubled beam in an effort to suppress the pedestal and improve the ICR. Data from second harmonic experiments are currently in process.

References

1. Semak, V.V., Thomas, J.G., and Campbell, B. R., (under review).
2. Nantel, M., Itatani, J., Tien, A., Faure, J., Kaplan, D., Bouvier, M., Buma, T., Van Rompay, P., Nees, J., Pronko, P. P., Umstadter, D. and Mourou, G. A., "Temporal Contrast in Ti: Sapphire Lasers: Characterization and Control," *IEEE Journal of Selected Topics in Quantum Electronics,* **vol. 4, no. 2**, pp. 449-458, 1998.
3. Curley, P. F., Darpentigny, G., Cheriaux, G., Chambaret, J. P. and Antonetti, A., "High dynamic range autocorrelation studies of a femtosecond Ti:sapphire oscillator and its relevance to the optimization of chirped pulse amplification systems," *Optics Communications,* **vol. 120**, pp. 71-77, 1995.
4. Braun, A., Rudd, J.V., Cheng, H., Mourou, G., Kopf, D., Jung, D., Weingarten, K.J., and Keller, U., "Characterization of short pulse oscillators by means of a high-dynamic-range autocorrelation measurement," *Optics Letters,* **vol. 20, no. 18**, pp. 1889-1891, 1995.
5. Knopolev, O., "Generation and Measurement of High Contrast Ultrashort Intense Laser Pulses," Dissertation, Departement of Mechanical Engineering, The College of Engineering and Applied Sciences, University of Rochester, 2000.
6. Furusawa, K., Takahashi, K., Kumagai, H., Midorikawa, K., and Obara, M., "Ablation characteristics of Au, Ag, and Cu metals using a femtosecond Ti:sapphire laser," *Journal of Applied Physics A: Materials Science & Processing,* **vol. A 69[Suppl.]**, pp. S359-S366, 1999.
7. Chichkov, B.N., Momma, C., Nolte, S., von Alvensleben, F., and Tunnermann, A., "Femtosecond, Picosecond, and Nanosecond Laser Ablation of Solids," *Journal of Applied Physics A: Materials Science and Processing*, **vol. 63**, pp. 109-115, 1996.
8. Wellershoff, S.S., Hohlfeld, J. and Matthias, J.G., "The role of electron-phonon coupling in femtosecond laser damage of metals," *Journal of Applied Physics A: Materials Science and Processing*, **A 69(Suppl.)**, S99-S107, 1999.
9. Corkum, P.B., Brunel, F., Sherman, N.K., and Shrinivasan-Rao, T., "Thermal Response of Metals to Ultrashort-Pulse Laser Excitation," *Physical Review Letters*, **vol. 61, no. 25**, pp. 2886-2889, 1988.
10. E. Hecht, *Optics*, 2nd ed., Addison Wesley, San Francisco, 2002.
11. Semak, V.V., Thomas, J.G., and Campbell, B. R., "Drilling of steel and HgCdTe with the femtosecond pulses produced by a commercial laser system," *Journal of Applied Physics D: Applied Physics*, **vol. 37**, pp. 2925-2931, 2004.
12. *Hurricane Integrated Ti:Sapphire Regenerative Amplifier System User's Manual*. Newport-Spectra Physics Corp., 2004.
13. *International Standard for Lasers and laser-related equipment-Test methods for laser beam parameters-beam widths, divergence angle, and beam propagation factor*, ISO 11146:1999(E), 1999.
14. Dausinger, F., "Femtosecond Technology for Precision Manufacturing: Fundamental and Technical Aspects," *Proceedings SPIE,* **vol. 4830**, pp. 471-478, 2003.
15. Nolte, S., Momma, C., Kamlage, G., Ostendorf, A., Fallnich, C., von Alvensleben, F., and Welling, H., "Polarization Effects in Ultrashort-pulse Laser Drilling," *Journal of Applied Physics A: Materials Science and Processing*, **vol. 68**, pp. 563-567, 1999.

Appendix A: Test Schedules

Table A.1. Percussion Drilling Test Schedule

Trial	Substrate Material	Substrate Thickness (mm)	Pulse Energy (μJ/pulse)	Environment
1	Stainless steel	0.076	211	Ambient
2			175	
3			140	
4			105	
5			70	
6			35	
7			211	Vacuum
8			175	
9			140	
10			105	
11			70	
12			35	
13	Stainless steel	0.127	211	Ambient
14			175	
15			140	
16			105	
17			70	
18			35	
19			211	Vacuum
20			175	
21			140	
22			105	
23			70	
24			35	
25	Stainless steel	0.254	281	Ambient
26			211	
27			175	
28			140	
29			105	
30			70	
31			281	Vacuum
32			211	
33			175	
34			140	
35			105	
36			70	

Table A.1. (Continued)

Trial	Substrate Material	Substrate Thickness (mm)	Pulse Energy (μJ/pulse)	Environment
37	Aluminum	0.051	175	Ambient
38			140	
39			105	
40			70	
41			35	
42			25	
43			175	Vacuum
44			140	
45			105	
46			70	
47			35	
48			25	
49	Aluminum	0.076	211	Ambient
50			175	
51			140	
52			105	
53			70	
54			35	
55			211	Vacuum
56			175	
57			140	
58			105	
59			70	
60			35	
61	Aluminum	0.127	211	Ambient
62			175	
63			140	
64			105	
65			70	
66			35	
67			211	Vacuum
68			175	
69			140	
70			105	
71			70	
72			35	

Table A.1. (Continued)

Trial	Substrate Material	Substrate Thickness (mm)	Pulse Energy (μJ/pulse)	Environment
73	Copper	0.127	211	Ambient
74			175	
75			140	
76			105	
77			70	
78			35	
79			211	Vacuum
80			175	
81			140	
82			105	
83			70	
84			35	
85	Copper	0.254	211	Ambient
86			175	
87			140	
88			105	
89			70	
90			35	
91			211	Vacuum
92			175	
93			140	
94			105	
95			70	
96			35	
97	Copper	0.406	351	Ambient
98			281	
99			211	
100			175	
101			140	
102			105	
103			351	Vacuum
104			281	
105			211	
106			175	
107			140	
108			105	

Table A.2. Test Schedule for Percussion Drilling at the Second Harmonic

Trial	Substrate Material	Substrate Thickness (mm)	Wavelength (nm)	Pulse Energy (μJ/pulse)	Environment
1	Aluminum	0.075	400	100	Ambient
2				90	
3				75	
4				60	
5				45	
6				35	
7				100	Vacuum
8				90	
9				75	
10				60	
11				45	
12				35	
13			800	100	Ambient
14				90	
15				75	
16				60	
17				45	
18				35	
19				100	Vacuum
20				90	
21				75	
22				60	
23				45	
24				35	

Appendix B: Substrate Legends

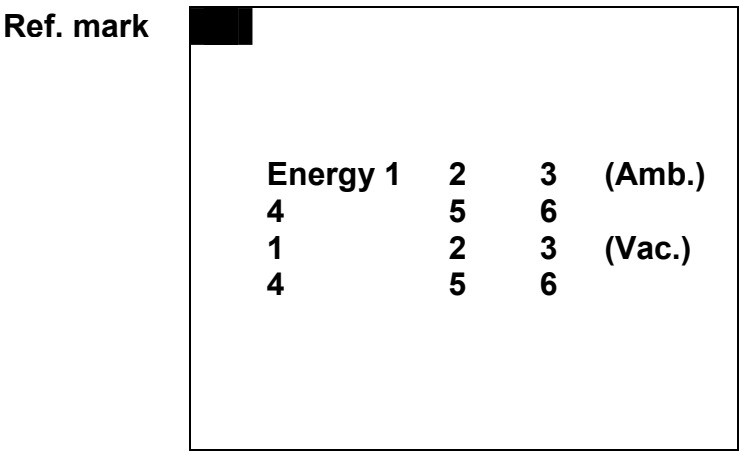

Fig. B.1. Substrate legend for percussion drilling experiments: each label designates the location of an array relative to the reference mark, run at the prescribed pulse energy.

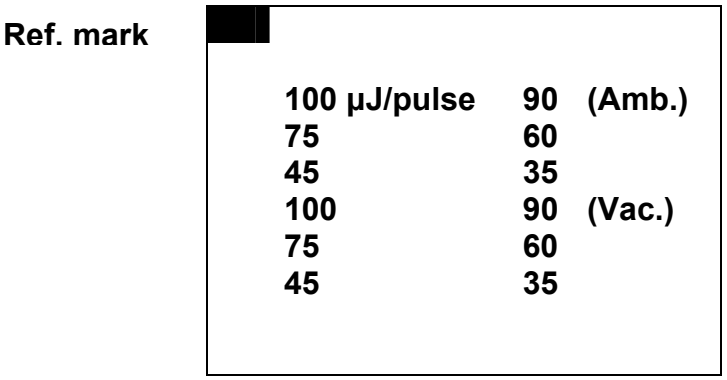

Fig. B.2. Substrate legend for percussion drilling experiments at the second harmonic: each label designates the location of an array relative to the reference mark, run at the indicated pulse energy.

Distribution

Copies	Name	Organization	MS/Address
2	Central Technical Files	08945-1	9960
2	Technical Library	04536	0899
1	WFO/CRADA Agreements	10112	0115
1	Tim Gardner	02455	1245
1	Pin Yang	02454	1245
1	Pennsylvania State University Electro Optics Center Attention: Jeff Thomas.		Electro-Optics Center 222 Northpointe Blvd. Freeport, PA 16229 (724) 295-7000, x7018